PRAMANA — journal of physics

Vol. 80, No. 3
March 2013
pp. 539–557

Real gauge singlet scalar extension of the Standard Model: A possible candidate for cold dark matter

ANIRBAN BISWAS* and DEBASISH MAJUMDAR
Astroparticle Physics and Cosmology Division, Saha Institute of Nuclear Physics, 1/AF Bidhan Nagar, Kolkata 700 064, India
Corresponding author. E-mail: anirban.biswas@saha.ac.in

MS received 8 February 2012; revised 18 August 2012; accepted 18 September 2012

Abstract. The simplest extension of Standard Model (SM) is considered in which a real SM gauge singlet scalar with an additional discrete symmetry Z_2 is introduced to SM. This additional scalar can be a viable candidate of cold dark matter (CDM) since the stability of S is achieved by the application of Z_2 symmetry on S. Considering S as a possible candidate of CDM, Boltzmann's equation is solved to find the freeze-out temperature and relic density of S for Higgs mass 120 GeV in the scalar mass range 5 GeV to 1 TeV. As HHSS coupling δ_2 appearing in Lagrangian depends upon the value of scalar mass m_S and Higgs mass m_h, the $m_S - \delta_2$ parameter space has been constrained by using the Wilkinson microwave anisotropy probe (WMAP) limit on the relic density of DM in the Universe and the results of recent ongoing DM direct search experiments, namely CDMS-II, CoGeNT, DAMA, EDELWEISS-II, XENON-10 and XENON-100. From such analyses, two distinct mass regions are found (a lower and higher mass domain) for such a DM candidate that satisfy both the WMAP limit and the experimental results considered here. The possible differential direct detection rates and annual variation of total detection rates have been estimated for this scalar DM candidate S for two detector materials, namely Ge and Xe. Finally, the γ-ray flux has been calculated from the galactic centre due to annihilation of two 130 GeV scalar DM into two monoenergetic γ-rays.

Keywords. Dark matter; beyond Standard Model.

PACS Nos 95.35.+d; 98.80.Cq

1. Introduction

In recent years, one of the most important areas of modern cosmology is the study of the existence and nature of dark matter (DM) in the Universe. The observations by Wilkinson microwave anisotropy probe (WMAP) [1] for studying the fluctuations in cosmic microwave background radiation reveal that the Universe consists of 27% matter and the rest 73% is an unknown energy known as dark energy. Only about 4% of matter accounts for ordinary matter such as leptons and baryons, gas, stars, galaxies, etc. The

rest (about 23%) of matter is completely unknown. Moreover, there are several cosmological observations such as rotation curves of spiral galaxies, gravitational microlensing, observations on Virgo [2] and Coma clusters [3], bullet clusters [4], etc. which provide indications of the existence of a huge amount of non-luminous matter or DM in the Universe.

Nature and identity of the constituents of DM are mostly unknown. However, evidences suggest that the DM candidates are mostly stable, non-baryonic, massive, non-relativistic particles having negligible or very weak interactions with other particles. These types of DM are often termed as cold dark matter (CDM) or weakly interacting massive particles (WIMP). In the early Universe, these particles would have been present in large numbers in thermal equilibrium. As the Universe expands and cools down, their density decreases resulting in the decrease of their interaction/annihilation rates. When the expansion rate of the Universe becomes larger than the annihilation rate of the WIMPs, they get decoupled from the Universe. Thus they 'freeze-out' from the other contents of the Universe and remain as relics. The temperature at which this phenomenon occurs is known as 'freeze-out' temperature and its density is called 'relic density'. After freeze-out, the relic density of WIMP is only affected by the expansion of the Universe. Since Standard Model (SM) of particle physics cannot provide any viable candidate for CDM, one has to consider theories beyond SM in order to explain the DM candidates (namely WIMP).

In this paper, we have considered the simplest possible renormalizable extension of SM by adding a real gauge singlet scalar S. We impose a discrete symmetry Z_2 on S and due to this symmetry, the additional scalar S is stable and can be a viable candidate for CDM. This model was first proposed by Silveira and Zee [5]. Thereafter, a number of authors have explored its phenomenology [6]. The relevance of the scalar singlet as a plausible candidate for DM is very elaborately described in ref. [7] and references therein. Investigating the relic density of a scalar DM by constraining the unknown parameters from direct detection experiments are addressed by previous authors. In ref. [8], the relic density is investigated for scalar singlet by constraining DM mass and direct detection rates from DAMA [9] results. Similar analysis including the CoGeNT [10] results and CDMS II [11] results are also addressed in ref. [12]. The analysis of scalar singlet DM scenario for XENON-100 [13] direct detection experiment results are also given in this reference. The scalar singlet DM with CoGeNT results are also discussed by Fitzpatrick *et al* [14]. The interpretation of Fermi Large Area Telescope (Fermi-LAT) results [15] with scalar singlet DM is discussed in ref. [16].

In the present work we estimate the freeze-out temperature and relic density of the DM candidate S by solving Boltzmann's equation. Then we constrain the parameter δ_2 [16a] by using WMAP limit on relic density of DM and the results of recent DM direct detection experiments such as CDMS-II [11,17], XENON-10 [18], XENON-100 [13], CoGeNT [10,19], EDELWEISS-II [20] and DAMA [9]. In CDMS and CoGeNT experiments, the target material is Ge and in XENON experiments, the target materials is Xe.

The constrained parameters thus obtained are then used to calculate the differential direct detection rates and the annual variation of total detection rates of the scalar DM candidate S for two detector materials, namely Ge and Xe. Therefore, we have calculated the γ-ray flux due to 130 GeV scalar DM for the annihilation channel $SS \rightarrow \gamma\gamma$ from the galactic centre.

The paper is organized as follows. In §2, we give a brief description of the scalar singlet model. Section 3 describes the formalism for computing relic abundance of a particular particle candidate. Results of the relic density calculations are given in §4. The model parameter δ_2 is constrained using the WMAP relic density data and the results obtained from various DM direct detection experiments. This is described in §5. The formalism for the calculation of direct detection rates and the annual variations of these rates are described in §6. With the constrained model parameter δ_2 as obtained in §5, the direct detection rates and the annual variations of total detection rates are calculated for this scalar DM candidate for some reference detector materials, namely Ge and Xe. The calculational procedure and the results are described in §7. In §8, we have calculated the γ-ray flux from galactic centre due to annihilation of DM present in the galactic halo. Finally in §9, we give a summary and conclusion.

2. The model

In the present work, we consider the simplest extension of SM where a real singlet scalar is added to the scalar sector of SM, and explore the possibility that it can be a candidate for CDM. The most general form of the potential appearing in the Lagrangian density for such a scalar fields is

$$V(H,S) = \frac{m^2}{2}H^\dagger H + \frac{\lambda}{4}(H^\dagger H)^2 + \frac{\delta_1}{2}H^\dagger H S + \frac{\delta_2}{2}H^\dagger H S^2 + \left(\frac{\delta_1 m^2}{2\lambda}\right)S + \frac{k_2}{2}S^2 + \frac{k_3}{3}S^3 + \frac{k_4}{4}S^4 \tag{1}$$

and the Lagrangian of this model is given by

$$\mathcal{L} = \mathcal{L}_{\rm SM} + \frac{1}{2}\partial_\mu S \partial^\mu S - \frac{\delta_1}{2}H^\dagger H S - \frac{\delta_2}{2}H^\dagger H S^2 - \left(\frac{\delta_1 m^2}{2\lambda}\right)S - \frac{k_2}{2}S^2 - \frac{k_3}{3}S^3 - \frac{k_4}{4}S^4, \tag{2}$$

where $\mathcal{L}_{\rm SM}$ is the SM Lagrangian, H is the SM Higgs doublet and S is the real gauge $(SU(2)_{\rm L} \times U(1)_{\rm Y})$ singlet scalar. The stability of S will be achieved by imposing a Z_2 symmetry ($S \to -S$, $\mathcal{L} \to \mathcal{L}$) over S. Therefore, under this symmetry, the coefficients of odd powers of S are zero (k_3 and δ_1 in eq. (2)). After spontaneous symmetry breaking, masses of the scalar field S and physical Higgs h are

$$m_{\rm S}^2 = k_2 + \delta_2 V^2/2, \tag{3}$$

$$m_{\rm h}^2 = -m^2 = \lambda V^2/2. \tag{4}$$

V is the VEV of Higgs ($V = 246$ GeV). In the present work, we have taken the mass $m_{\rm S}$ of the scalar particle S in the range 5 GeV–1 TeV. Depending on its mass, the DM candidate S annihilates into fermion pairs, gauge boson pairs and Higgs pairs.

3. Formalism for the calculation of relic abundance

In order to calculate the relic abundance of the scalar particle S, we have solved numerically the Boltzmann's equation which is given by

$$\frac{\mathrm{d}n}{\mathrm{d}t} + 3Hn = -\langle\sigma v\rangle(n^2 - n_{\mathrm{eq}}^2), \tag{5}$$

where n is the number density of the scalar particle S and n_{eq} is the value of n when S was in equilibrium (when temperature $T > T_{\mathrm{f}}$, T_{f} is the freeze-out temperature of S), H denotes the Hubble parameter, $\langle\sigma v\rangle$ is the thermal average of the product of annihilation cross-section and the relative velocity of the two annihilating particles (in this case, the scalar singlet S). It is useful to define two dimensionless quantities, $Y = n/s$ [21] and $x = m/T$, where s is the total entropy density of the Universe and T is the photon temperature. From the standard Friedmann–Robertson–Walker cosmology, the Hubble parameter $H = \sqrt{\frac{8}{3}\pi G\rho}$ where G is the gravitational constant. The total energy density ρ and the total entropy density s of the Universe are given by [21]

$$\rho = g_{\mathrm{eff}}(T)\frac{\pi^2}{30}T^4 \tag{6}$$

and

$$s = h_{\mathrm{eff}}(T)\frac{2\pi^2}{45}T^3. \tag{7}$$

In eqs (6) and (7), g_{eff}, h_{eff} are the effective degrees of freedom for the energy and entropy densities. Substituting eqs (6) and (7) and the expression of H into eq. (5), we arrive at the equation for the evolution of Y as

$$\frac{\mathrm{d}Y}{\mathrm{d}x} = -\left(\frac{45}{\pi}G\right)^{-1/2}\frac{g_*^{1/2}m}{x^2}\langle\sigma v\rangle(Y^2 - Y_{\mathrm{eq}}^2), \tag{8}$$

where $g_*^{1/2}$ is defined as [21]

$$g_*^{1/2} = \frac{h_{\mathrm{eff}}}{g_{\mathrm{eff}}^{1/2}}\left(1 + \frac{1}{3}\frac{T}{h_{\mathrm{eff}}}\frac{\mathrm{d}h_{\mathrm{eff}}}{\mathrm{d}T}\right). \tag{9}$$

Y_{eq} is the value of Y when $n = n_{\mathrm{eq}}$. The expression for Y_{eq} is given by [21]

$$Y_{\mathrm{eq}} = \frac{45g}{4\pi^4}\frac{x^2K_2(x)}{h_{\mathrm{eff}}(m/x)}, \tag{10}$$

where g is the number of internal degrees of freedom of the species under consideration (here $g = 1$), m is the mass and $K_n(x)$ is the modified Bessel function of order n. From eqs (8) and (10), we obtain

$$\left(\frac{45}{\pi}G\right)^{-1/2}\frac{45g}{4\pi^4}\frac{K_2(x)}{h_{\mathrm{eff}}(T)}g_*^{1/2}m\langle\sigma v\rangle\delta(\delta+2) = \frac{K_1(x)}{K_2(x)} - \frac{1}{x}\frac{\mathrm{d}\ln h_c(T)}{\mathrm{d}\ln T}. \tag{11}$$

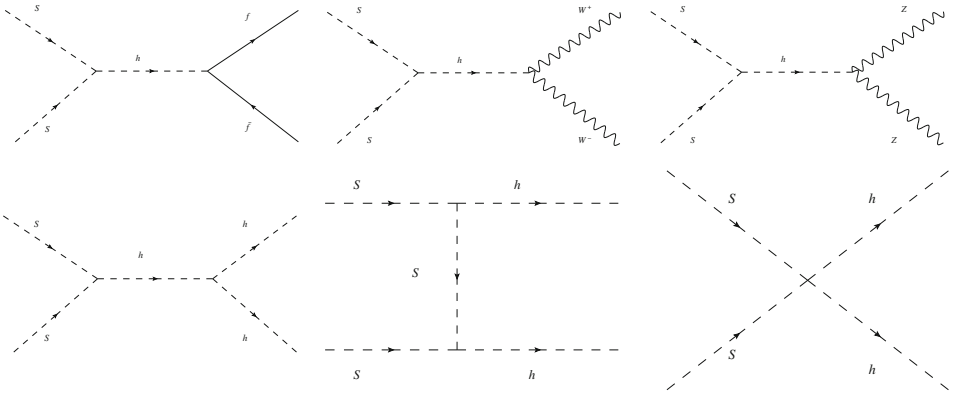

Figure 1. Lowest order Feynman diagrams of two S annihilate into a pair of fermion and antifermion, W^+W^-, ZZ and Higgs.

In the above equation, $h_c(T)$ is the contribution to $h_{\text{eff}}(T)$ from all species which are coupled to the Universe at temperature T. Equation (11) is solved numerically in a self-consistent manner in order to obtain the value of x_{f} (and hence the freeze-out temperature T_{f} $(= m/x_{\text{f}})$). In the present case, we have taken the value of δ to be 1.5 [21]. Integrating eq. (8) from $x = x_0 = m/T_0$ to $x = x_{\text{f}} = m/T_{\text{f}}$, where T_0 is the present photon temperature, which is of the order of 10^{-14} GeV (~ 0), we obtain Y_0 (value of Y at $T = T_0$). Knowing Y_0, we can compute the relic density of the DM candidate (here S) from the relation [21],

$$\Omega h^2 = 2.755 \times 10^8 \text{ m/GeV} \times Y_0. \tag{12}$$

In the above equation, $\Omega = \rho/\rho_{\text{c}}$ (ρ being the DM density and ρ_{c} is the critical density of the Universe) and $h = H/(100\,\text{km s}^{-1}\,\text{Mpc}^{-1})$.

The expressions for annihilation cross-section $\langle \sigma v \rangle$ for processes such as $SS \to f\bar{f}, W^+W^-, ZZ, hh$ are given in refs [22,23] and the Feynmann diagrams for these processes are shown in figure 1. In this work, we consider Higgs mass value m_{h} as 120 GeV. The variations of annihilation cross-sections with scalar DM mass m_{S} are shown in figure 2a for different values of δ_2.

4. Calculational procedure and results

The relic density for scalar DM is obtained after an elaborate computation. We first calculate the freeze-out temperature T_{f} for scalar DM with different values of coupling constant δ_2 and mass m_{S}. For this purpose, we have solved eq. (11) numerically. The values of the quantities $g_*^{1/2}$, $g_{\text{eff}}^{1/2}$ and h_{eff} for different T required for solving eq. (11), are obtained from the figures (for the QCD phase transition temperature of 150 MeV) given in refs [21,24]. In figure 2b, representative plots are the variations of T_{f} in the scalar DM mass range of 5 GeV to 1 TeV for different values of δ_2 ($\delta_2 = 0.05$, 0.1, 0.7) and $m_{\text{h}} = 120$ GeV, the topmost plot is for the lowest value of δ_2 considered and the plots below are for

other considered values of δ_2 in the increasing order. In general, the freeze-out temperature T_f is approximately given by $T_f \sim m_S/20$. The plot for $T_f = m_S/20$ is also shown in figure 2b (black line) for reference. The sudden dip in the values for T_f in figure 2b around $m_S = 60$ GeV can be understood from the expression of $\langle \sigma v \rangle_{f\bar{f}}$ (given in refs [22,23]). At this point, there is a sudden rise in $\langle \sigma v \rangle$ (figure 2a) and it is due to Higgs propagator appearing in the annihilation process ($SS \to f\bar{f}$). Using the values of freeze-out temperatures (calculated from eq. (11)) in eq. (12), the relic densities of the scalar DM for different scalar DM masses and different values of δ_2 are computed. The results are shown in figure 3. In figure 3, the two parallel lines denote the WMAP limits on relic density of DM ($0.099 \leq \Omega h^2 \leq 0.123$). The different plots in figure 3 correspond to

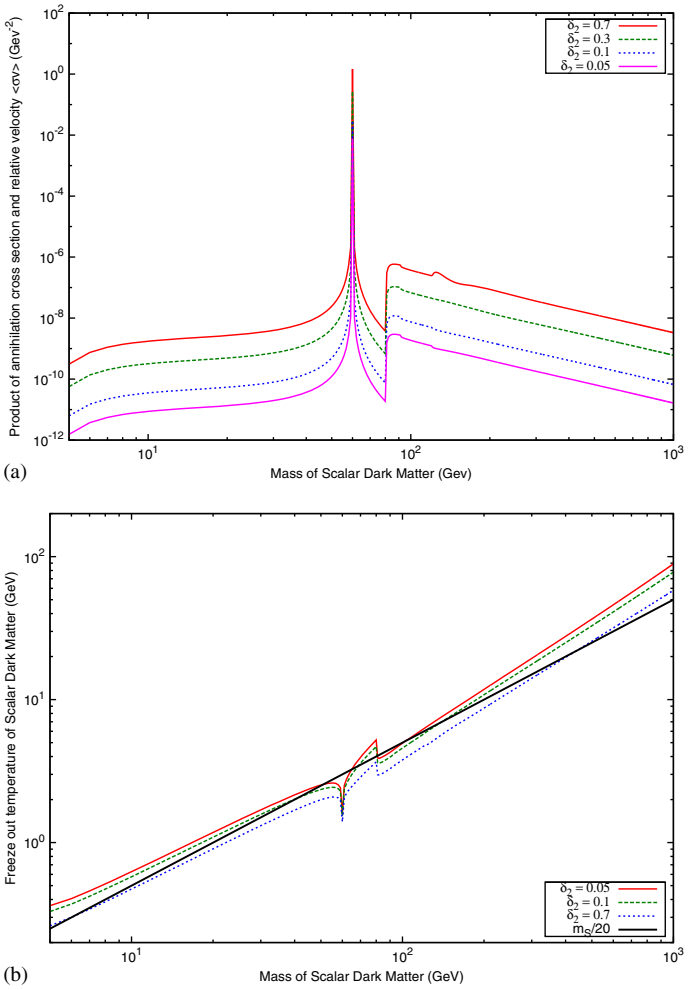

Figure 2. (**a**) Variation of product of annihilation cross-section and relative velocity $\langle \sigma v \rangle$ with the mass of scalar DM S for $\delta_2 = 0.7, 0.3, 0.1, 0.05$; (**b**) Variation of freeze-out temperature T_f with the mass for $\delta_2 = 0.7, 0.1, 0.05$.

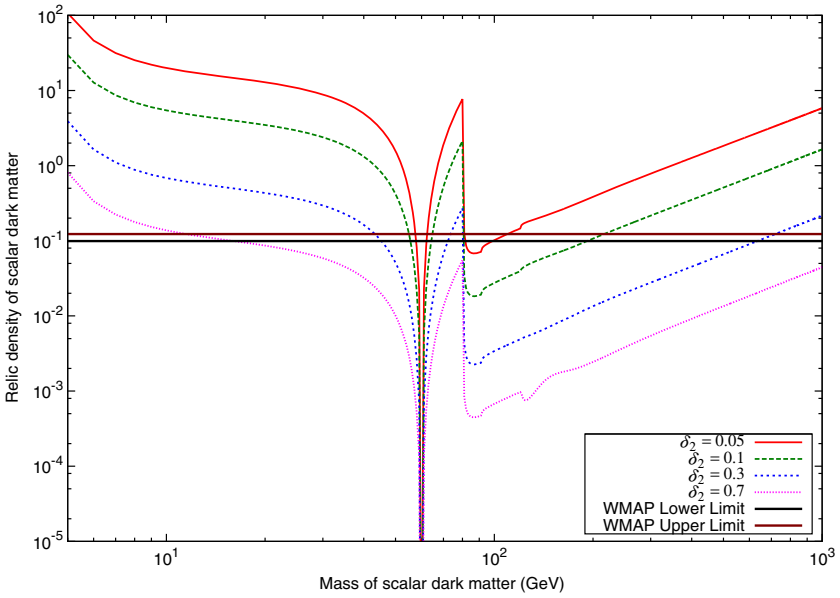

Figure 3. Variation of relic density Ωh^2 with the mass of scalar DM for Higgs mass = 120 GeV.

different values of δ_2, namely $\delta_2 = 0.05, 0.1, 0.3, 0.7$, respectively; the topmost one is for the smallest value of δ_2 considered and the successive lower plots are for the other considered values of δ_2 in increasing order. We have seen from figure 2a that initially the annihilation cross-section of S increases with m_S; then at $m_S \approx m_h/2$, $\langle \sigma v \rangle$ rises rapidly and after which it decreases with the increase of m_S. Again for $m_S \sim 81$ GeV, $\langle \sigma v \rangle$ suddenly increases up to nearly two orders of magnitudes from its value at $m_S \sim 80$ GeV and it is due to the fact that for $m_S > 80.4$ GeV, the annihilation channel $SS \to W^+W^-$ becomes kinematically possible. Thereafter, $\langle \sigma v \rangle$ starts decreasing with the increase of m_S. Since relic density is inversely proportional to $\langle \sigma v \rangle$ [23a], the variation of relic density of DM particle S with m_S is just opposite to the variation $\langle \sigma v \rangle$ with m_S. This feature is reflected in figure 3. Also, since $\langle \sigma v \rangle$ is directly proportional to δ_2^2 and its higher powers, higher the value of δ_2, lower is the value of relic density (figure 3).

5. Constraining the model parameter δ_2

The model parameter δ_2 is a very important parameter for the present model because it appears in both the expressions of annihilation and scattering cross-section of scalar DM S. The spin-independent scattering cross-section for scalar DM S is given later in eq. (13). In this section, we have constrained the parameter space $(m_S - \delta_2)$ by using WMAP limit on relic density of DM and the results of recent experiments such as CoGeNT, DAMA, CDMS-II, XENON-10, XENON-100 and EDELWEISS-II. Similar to the previous discussions, here also we perform the calculations for Higgs mass $m_h = 120$ GeV with m_S

in the range 5 GeV $\leq m_S \leq$ 1 TeV. The results obtained are shown in figure 4. We first use the WMAP limit ($0.099 \leq \Omega h^2 \leq 0.123$) on relic density of DM and using that limit we get the allowed values of m_S for each value of δ_2 (from figure 3). These results are shown in figure 4 using turquoise-coloured contour. Thereafter, we estimate the allowed values of δ_2 and m_S using the mass–cross-section limits given by the experiments such as CDMS-II, DAMA, CoGeNT, XENON-10, XENON-100, EDELWEISS-II and eq. (13). In figure 4, the magenta-coloured contour represents the allowed region of scalar DM S obtained from CoGeNT data (2010) [10]. The overlap region between these contours (magenta and turquoise) is therefore satisfied by both WMAP and CoGeNT (2010) results. From the overlap region (figure 4), the range of m_S (in GeV) is found to be $7.7 \leq m_S \leq 11.15$ and the corresponding range of coupling δ_2 is obtained as $0.7 \leq \delta_2 \leq 0.95$. These ranges therefore satisfy both WMAP and CoGeNT (2010) limits. The dark blue-coloured contour indicates (figure 4) new bounds from CoGeNT data (2011) [19]. The common region between CoGeNT (2011) and WMAP lies in the range $8.0 \leq m_S \leq 8.53$ GeV, $0.8 \leq \delta_2 \leq 0.9$. This common intersection region is also well-supported by CoGeNT (2010) and CDMS-II (2010) data [25] (purple dashed line).

Similar $m_S - \delta_2$ contours obtained from the DAMA experiment results (with channelling) are shown as maroon contours in figure 4. One sees that the small overlap region between the two contours (turquoise and maroon) is restricted by the scalar mass (in GeV) range $14.8 \leq m_S \leq 15.9$. The corresponding values of δ_2 are found to be around 0.6. We remark in the passing that we have checked for other allowed regions in 'DM mass–$\sigma^{\text{scalar}}_{\text{nucleon}}$' plane given by DAMA experiment, but we have not obtained any overlap region such as described above. One such region (maroon-coloured contour) is also

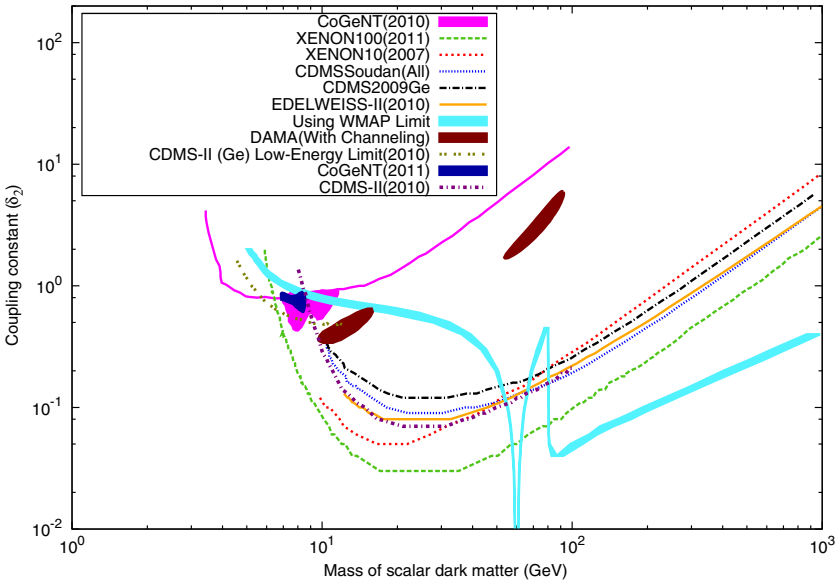

Figure 4. Constraining the parameter space (m_S–δ_2) of scalar DM for Higgs mass 120 GeV by using WMAP limit and recent experimental results of CDMS-II, XENON-10, XENON-100, CoGeNT, DAMA and EDELWEISS-II.

shown in figure 4. The olive dashed line in figure 4 represents upper bounds that we have obtained from low-energy analysis of the CDMS-II germanium data [17]. But, it has no intersection with WMAP satisfied region (turquoise-coloured contour).

Unlike CoGeNT and DAMA, other experiments such as XENON-10, XENON-100, CDMS-II and EDELWEISS-II do not provide a bounded allowed region in m_S–σ_N plane (σ_N is the scattering cross-section of DM and nucleon). Instead they provide upper bounds of scattering cross-section for a particular mass of DM. Consequently, we also obtain upper bound of δ_2 for a specific mass of S for those experiments. These results are also shown in figure 4. In figure 4, green dashed line represents the upper bound of δ_2 for XENON-100. CDMS-II results (CDMS 2009 Ge and CDMS Soudan (All) (which are results obtained by CDMS-II Collaboration from the combined analysis of full dataset of Soudan)) are shown by black and blue dashed lines. XENON-10 and EDELWEISS-II results are represented by red dashed and orange solid lines, respectively. The WMAP results (turquoise plot in figure 4) intersect with the upper bounds obtained from XENON-10 results in m_S–δ_2 plane are found to be at the values of $m_S = 53.5$, $\delta_2 = 0.12$, $m_S = 67.4$, $\delta_2 = 0.16$ and $m_S = 80.2$, $\delta_2 = 0.21$. Therefore, the turquoise region below ($m_S = 53.5$, $\delta_2 = 0.12$), ($m_S = 67.4$, $\delta_2 = 0.16$) and ($m_S = 80.2$, $\delta_2 = 0.21$) is obeyed by both WMAP and XENON-10. Similarly, the regions satisfied by both CDMS-II results (CDMS 2009 Ge, CDMS Soudan (All)) and WMAP are represented by turquoise coloured line below the intersection points ($m_S = 52.0$, $\delta_2 = 0.15$), ($m_S = 67.9$, $\delta_2 = 0.17$), ($m_S = 80.3$, $\delta_2 = 0.20$) and ($m_S = 53.9$, $\delta_2 = 0.12$), ($m_S = 66.5$, $\delta_2 = 0.14$), ($m_S = 80.4$, $\delta_2 = 0.16$), respectively as shown in figure 4. Also the overlap regions of WMAP, XENON-100 and WMAP, EDELWEISS-II below the following intersection points, can be read out from figure 4 as ($m_S = 57.6$, $\delta_2 = 0.05$), ($m_S = 62.5$, $\delta_2 = 0.05$), ($m_S = 80.5$, $\delta_2 = 0.07$) and ($m_S = 54.1$, $\delta_2 = 0.11$), ($m_S = 66.7$, $\delta_2 = 0.14$), ($m_S = 80.4$, $\delta_2 = 0.17$). We have also found that for XENON-100, there is another intersection point with WMAP in the lower mass region around $m_S \sim 6.0$ GeV, $\delta_2 \sim 1.25$.

From the above analyses, it appears that there are two distinct regions in the m_S–δ_2 plane for scalar DM S, which are the allowed regions for both WMAP and recent experiments. The regions can be classified as follows:

(1) A lower mass region where we have found three mass ranges for scalar DM S: These ranges are given by $m_S \sim 6$ GeV ($\delta_2 \sim 1.25$), 7.7 GeV $\leq m_S \leq$ 11.15 GeV ($0.7 \leq \delta_2 \leq 0.95$) and 14.8 GeV $\leq m_S \leq$ 15.9 GeV ($\delta_2 \sim 0.6$). The corresponding ranges for coupling δ_2 which we have found are given within brackets. This lower mass domain is supported by WMAP and various ongoing DM direct detection experiments. In this case $m_S \sim 6$ GeV is supported by WMAP and XENON-100. Second and third mass ranges are obeyed by WMAP, CoGeNT (2010) data and WMAP, DAMA (with channelling) data, respectively (figure 4).

But if we use more recent data of CoGeNT (CoGeNT (2011) data), then the second mass range of scalar DM S gets reduced to 8.0 GeV $\leq m_S \leq$ 8.53 GeV. The ranges for coupling δ_2 are also reduced to $0.8 \leq \delta_2 \leq 0.9$. It is also seen from figure 4 that this region is supported by CDMS-II (2010) bounds. Other mass ranges remain unchanged.

(2) A higher mass region with the scalar DM mass range $\sim$52.5 GeV $\leq m_S \leq$ $\sim$1000 GeV, with the range of δ_2 is found as $0.02 \leq \delta_2 \leq 0.4$ (figure 4): This mass

region is satisfied by the allowed domains of WMAP, CDMS-II, EDELWEISS-II, XENON-10 and XENON-100.

Here we make some comments about the region of the parameter space (m_S vs. δ_2) that is not satisfied by the results of the direct detection experiments we have considered. In this region (15 GeV $< m_S <$ 52.5 GeV), the values of δ_2 required to obtain current relic density (within WMAP limit) are such that the scattering cross-sections obtained using these values for different DM masses do not satisfy the experimental limits given by different exclusion plots.

6. Formalism for the calculation of direct detection rates

In this section, we estimate the differential direct detection rates and their annual variations for scalar DM S. For this purpose, we have chosen ^{76}Ge and ^{131}Xe as detector materials. The direct detection of DM by a terrestrial detector uses the principle of elastic scattering of DM particles off the detector nuclei and the energy of the recoil nucleus is measured. It is very difficult to measure the low recoil energy of nuclei accurately and hence a very low threshold and low background detector is required. In figure 5, we show the Feynman diagram for such an elastic scattering process of scalar singlet S through Higgs exchange. The scalar singlet S-nucleon N elastic scattering ($SN \to SN$) cross-section [26] is given by

$$\sigma_{\mathrm{N}}^{\mathrm{scalar}} = \frac{\delta_2^2 v^2 |\mathcal{A}_{\mathrm{N}}|^2}{4\pi} \left(\frac{m_{\mathrm{r}}^2}{{M_{\mathrm{S}}}^2 {M_{\mathrm{h}}}^4} \right), \tag{13}$$

where $m_{\mathrm{r}}(N, S) = M_{\mathrm{N}} M_{\mathrm{S}}/(M_{\mathrm{N}} + M_{\mathrm{S}})$ is the reduced mass, $\mathcal{A}$ is the coupling between Higgs and nucleon N and its value is ~ 340 MeV/V [26], with V being the VEV of Higgs boson. The scalar singlet-nucleus elastic scattering cross-section is given by [26]

$$\sigma_{\mathrm{nucleus}}^{\mathrm{scalar}} = \frac{A^2 \mathrm{m}_{\mathrm{r}}^2(\mathrm{nucleus}, S)}{\mathrm{m}_{\mathrm{r}}^2(\mathrm{nucleon}, S)} \sigma_{\mathrm{nucleon}}^{\mathrm{scalar}}. \tag{14}$$

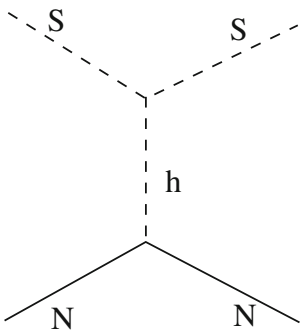

Figure 5. Feynman diagram for the elastic scattering between S and nucleon N via Higgs exchange.

In the above equation, A is the mass number of the nucleus. The differential detection rate of DM per unit detector mass is given by [27]

$$\begin{aligned}\frac{\mathrm{d}R}{\mathrm{d}E_{\mathrm{R}}} &= \frac{\sigma^{\mathrm{scalar}}_{\mathrm{nucleus}}\rho_{\mathrm{S}}}{4v_{\mathrm{e}}m_{\mathrm{S}}m_{\mathrm{r}}^2}F^2(E_{\mathrm{R}}) \\ &\quad\times\left[\mathrm{erf}\left(\frac{v_{\mathrm{min}}+v_{\mathrm{e}}}{v_0}\right)-\mathrm{erf}\left(\frac{v_{\mathrm{min}}-v_{\mathrm{e}}}{v_0}\right)\right] \\ &= T_1T_2T_3, \end{aligned} \tag{15}$$

where

$$\begin{aligned} T_1 &= \frac{\sigma^{\mathrm{scalar}}_{\mathrm{nucleus}}\rho_{\mathrm{S}}}{4v_{\mathrm{e}}m_{\mathrm{S}}m_{\mathrm{r}}^2}, \qquad T_2 = F^2(E_{\mathrm{R}}), \\ T_3 &= \left[\mathrm{erf}\left(\frac{v_{\mathrm{min}}+v_{\mathrm{e}}}{v_0}\right)-\mathrm{erf}\left(\frac{v_{\mathrm{min}}-v_{\mathrm{e}}}{v_0}\right)\right], \end{aligned} \tag{16}$$

where v_{e} is the velocity of Earth with respect to the galactic frame of reference. Its expression is given by [27],

$$v_{\mathrm{e}} = v_{\odot} + v_{\mathrm{orb}}\cos\gamma\cos\left(\frac{2\pi(t-t_0)}{T}\right). \tag{17}$$

In the above expression, t denotes any time of the year, $T = 1$ year is the time period of Earth's motion around the Sun, $v_{\mathrm{orb}} = 30$ km/s is the Earth's orbital speed and $\gamma \backsimeq 60^\circ$ is the angle subtended by the ecliptic at the galactic plane. The solar velocity $v_{\odot}$ is given by

$$v_{\odot} = v_0 + v_{\mathrm{pec}}, \tag{18}$$

where v_0 is the circular speed of Sun around the galactic centre which is taken to be 220 km/s and v_{pec} is the peculiar velocity with $v_{\mathrm{pec}} = 12$ km/s. The periodicity in eq. (17) causes an annual modulation of the event rates of DM in a terrestrial detector which serve as a definite signal of DM detection. In the eq. (15), $F(E_{\mathrm{R}})$ is the nuclear form factor given by ref. [28], ρ_{S} is the DM density in the solar neighbourhood, which is equal to 0.3 GeV/cm^3 for the rest of our calculations in this section. v_{min} denotes the minimum velocity of DM required to produce a recoil energy E_{R}. The expression of v_{min} is given by

$$v_{\mathrm{min}} = \left(\frac{m_{\mathrm{nucleus}}E_{\mathrm{R}}}{2m_{\mathrm{r}}^2}\right)^{1/2}. \tag{19}$$

The measured response of the detector by the scattering of DM off the detector nucleus is in fact a fraction of the actual recoil energy. Thus, the actual recoil energy E_{R} is quenched by a factor q_X (different for different nucleus X) and we should express differential rate in eq. (15) in terms of $E = q_X E_{\mathrm{R}}$. Thus, the differential detection rate (events/kg/day/keV) in terms of the observed recoil energy E for a monoatomic detector such as Xe can be expressed as

$$\frac{\Delta R}{\Delta E}(E) = \int_{E/q_{\mathrm{Ge}}}^{(E+\Delta E)/q_{\mathrm{Xe}}}\frac{\mathrm{d}R_{\mathrm{Xe}}}{\mathrm{d}E_{\mathrm{R}}}(E_{\mathrm{R}})\frac{\mathrm{d}E_{\mathrm{R}}}{\Delta E}. \tag{20}$$

The total detection rate of DM is obtained by integrating eq. (15) as

$$R = \int_{E_T}^{\infty} \frac{dR}{dE_R} dE_R, \tag{21}$$

where E_T is the threshold energy for a given detector material.

7. Direct detection rates for scalar DM

In the present work, computations of direct detection rates are performed with $m_h = 120$ GeV, $\Delta E = 0.5$ keV and at a time $t = t_0$. As discussed earlier, we have computed the direct detection rates and their annual variations for each of the detector materials, namely ^{76}Ge and ^{131}Xe. The quenching factors for ^{76}Ge = 0.25 [29] and ^{131}Xe = 0.8 [29]. The differential detection rates and their annual variations can now be computed using eqs (15)–(21).

The variation of differential detection rates of scalar DM S with observed recoil energy E for monoatomic targets such as Xe and Ge are shown in figure 6. In figure 6a, we show the estimates of differential detection rates for different values of observed recoil energy E, with Xe as target material for $m_S = 55$ GeV (red solid line) and $m_S = 65$ GeV (green solid line). For both the cases, the value of the coupling constant δ_2 is taken to be 0.1 (in agreement with the higher mass region described in §5). Figure 6a shows that although the two plots corresponding to two scalar masses are distinguishable at lower recoil energies ($\leq$11 keV), at higher recoil energies they tend to coincide. In figure 6b, we show the direct detection rate results for Ge. In this case, calculations are performed for two sets of $m_S - \delta_2$ values, namely $m_S = 10$ GeV, $\delta_2 = 0.8$ and $m_S = 8$ GeV, $\delta_2 = 0.9$. These values are chosen from the allowed lower mass domain discussed in §5 (figure 4). It is seen from figure 6b that the rates for the set ($m_S = 8$ GeV, $\delta_2 = 0.9$, represented by green solid line), falls off faster than those for the set ($m_S = 10$ GeV, $\delta_2 = 0.8$, represented by red solid line). The nature of $\Delta R/\Delta E$ for Xe (figure 6a) can be explained by examining the variation of T_3 (eq. (16)) with E. This is shown in figure 7a. For low values of E and high mass range of S ($m_S \gtrsim 55$ GeV), v_{min} (eq. (19)) $\ll v_e$ and hence T_3 is effectively independent of E. Therefore, as E increases, the values of T_3 for $m_S = 65$ GeV becomes larger than those for $m_S = 55$ GeV. Also, $\sigma^{scalar}_{nucleus}$ is inversely proportional to m_S and T_1 is directly proportional to $\sigma^{scalar}_{nucleus}$. Consequently, T_1 is inversely proportional to m_S. Now the variation of $\Delta R/\Delta E$ with E is due to the combined effects of both T_1 and T_3 (eq. (15)). This explains the nature of the plots for Xe in figure 6. In the case of Ge however, T_1 is nearly the same for both the masses considered. Consequently, the variations of $\Delta R/\Delta E$ with E (figure 6b) are dominated only by the nature of variations of T_3 with E. These variations are shown in figure 7b, which explains the nature of variations of $\Delta R/\Delta E$ with E for Ge.

The annual variations of the total detection rates of WIMP are a crucial evidence for DM. This variation is caused by the periodic motion of Earth around the Sun in which the directionality of Earth's motion changes over the year. Since the solar system moves towards the direction of Cygnus constellation, Earth experiences a WIMP wind apparently coming from the direction of Cygnus. Due to the periodic motion of Earth, the relative speed between Earth and WIMP changes over the year. It becomes maximum

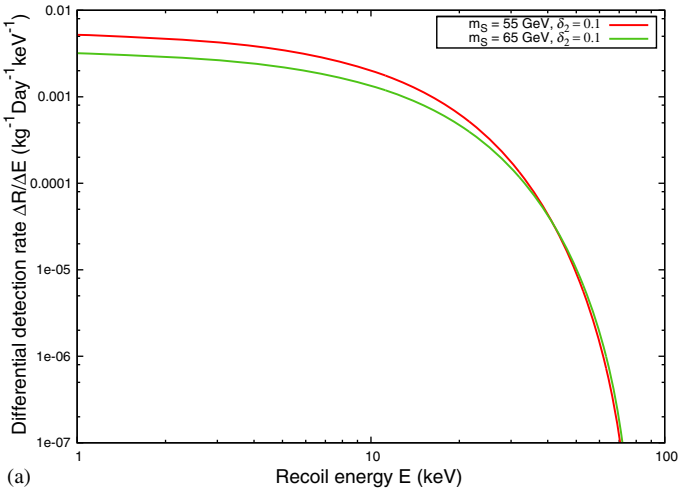

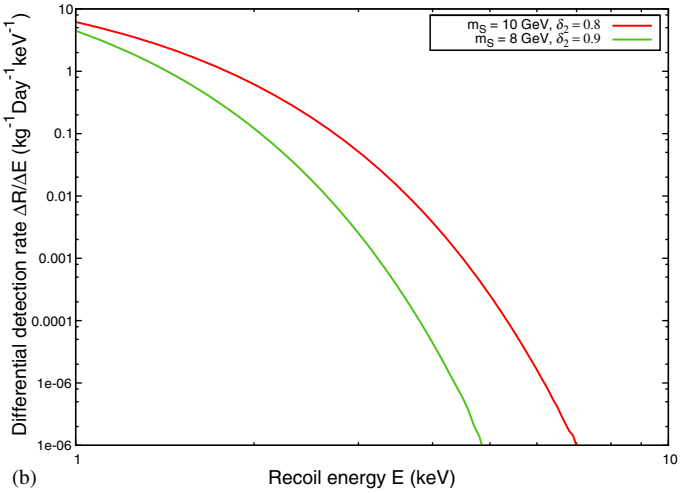

Figure 6. Variation of differential detection rates $\Delta R/\Delta E$ of scalar DM S with observed recoil energy E for monoatomic detectors Xe (**a**) and Ge (**b**).

when velocities of both the solar system and Earth are in the same direction (on 2 June) in which case the Earth encounters maximum WIMP flux. The WIMP flux encountered by the Earth is minimum when velocities of Earth and Sun are in opposite directions. Consequently, maximum events are expected on 2 June of every year.

In this work, we compute the total detection rates at each day of a year, for the same detector materials, namely Xe and Ge, considering the scalar singlet as DM candidate. The results are then plotted with the days of the year which show the annual variation of total detection rates. The calculations for Xe are performed for the set ($m_S = 55$ GeV, $\delta_2 = 0.1$), whereas for Ge, the set ($m_S = 10$ GeV, $\delta_2 = 0.8$). The results for Xe and Ge are shown in figures 8a and 8b respectively. All the plots in figure 8 show that the maximum expected events are at $t = 153$ (day) (corresponding to 2 June).

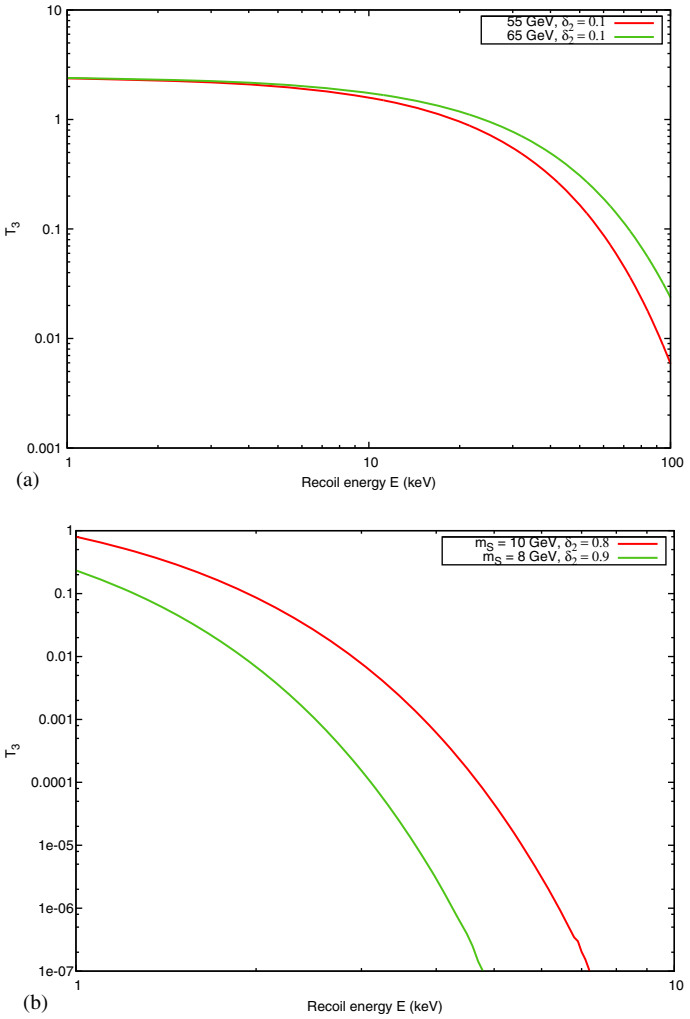

Figure 7. (**a**) Variation of T_3 with observed recoil energy E for Xe with $m_S = 55$ GeV (green solid line), 65 GeV (red solid line). (**b**) Same for Ge with $m_S = 10$ GeV (red solid line), 8 GeV (green solid line).

8. Indirect detection of scalar DM

Another promising method for the detection of DM (WIMPs) is the observation of annihilation products of DM present in the galactic halo. In this section, we shall consider γ-rays coming from the DM annihilation in the galactic centre (GC).

Recently, it has been reported that there is a 4.6σ (3.3σ) [30,31] local (global) evidence of a monochromatic γ-ray line with an energy $E_\gamma \approx 130$ GeV by the publicly available data [32] of Fermi-LAT. This signal comes from two regions, one of which is nearly at the centre of our galaxy ($-1°$, $-0.7°$), hereinafter referred to as the 'central region' and another is located at ($-10.0°$, $-0.0°$), called the 'west region'. Both regions are extended

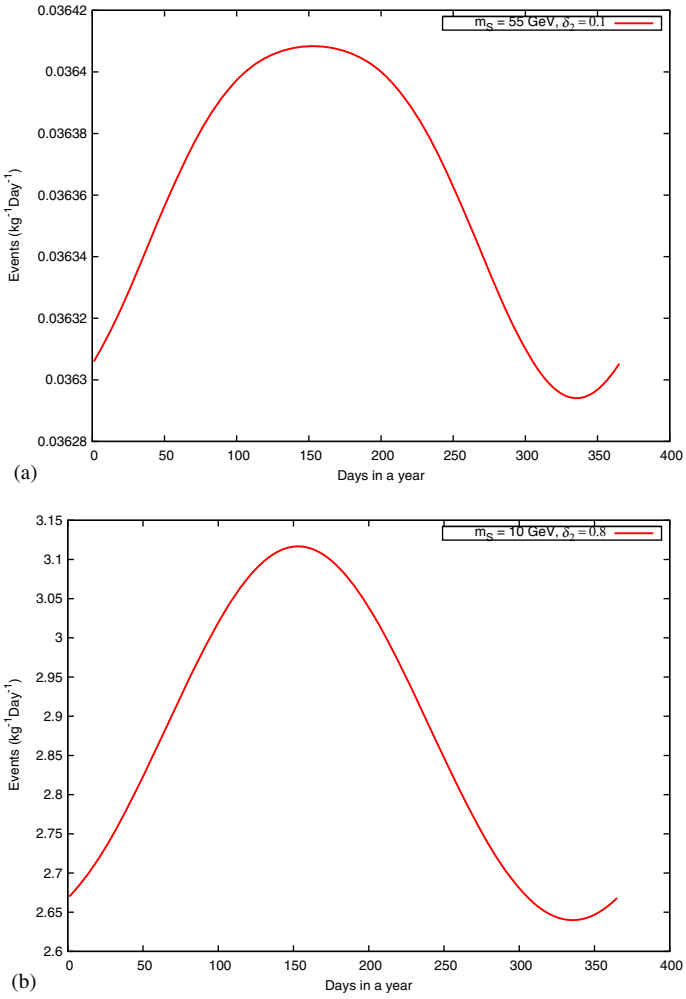

Figure 8. (**a**) Annual variation of total detection rates of scalar DM for Xe (monoatomic target) with $m_S = 55$ GeV, $\delta_2 = 0.1$. (**b**) Same for Ge with $m_S = 10$ GeV, $\delta_2 = 0.8$.

within a circle of radius of 3°. It is suggested that this excess of γ-ray signals from galactic centre is not associated with the Fermi bubbles [31] and may result from DM annihilation into two monochromatic γ-rays.

We have calculated the γ-ray flux due to 130 GeV scalar DM annihilation in the 'central region' of our Milky Way Galaxy. The Feynman diagram for the process $SS \to \gamma\gamma$ is shown in figure 9.

The expression of γ-ray flux due to DM annihilation in galactic halo is given in ref. [33],

$$\frac{\mathrm{d}\Phi_\gamma}{\mathrm{d}E_\gamma} = \frac{1}{8\pi}\frac{\langle\sigma v\rangle_{SS\to\gamma\gamma}}{m_S^2}\frac{\mathrm{d}N_\gamma}{\mathrm{d}E_\gamma} r_\odot \rho_\odot^2 J, \tag{22}$$

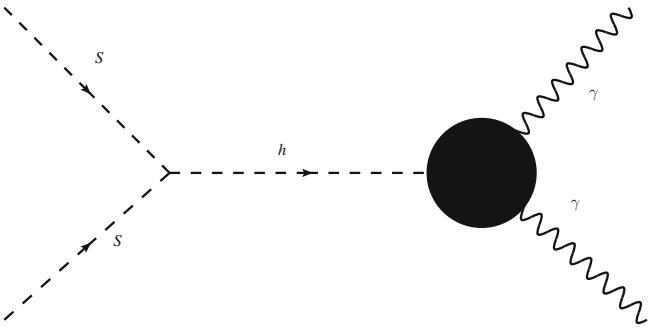

Figure 9. Feyman diagram for the process $SS \to \gamma\gamma$.

where

$$J = \int \mathrm{d}b \int \mathrm{d}l \int_{\text{l.o.s}} \frac{\mathrm{d}s}{r_\odot} \cos b \left(\frac{\rho(r)}{\rho_\odot}\right)^2 \tag{23}$$

and

$$\frac{\mathrm{d}N_\gamma}{\mathrm{d}E_\gamma} = 2\delta(E - E_\gamma). \tag{24}$$

In the above equation, l and b are the galactic longitude and latitude, respectively. We have performed l, b integration (in eq. (23)) over the 'central region' of our galaxy and the s integration (in eq. (23)) along the line of sight (l.o.s). Relation between r and s is given by

$$r = (s^2 + r_\odot^2 - 2sr_\odot \cos l \cos b)^{1/2}, \tag{25}$$

where $r_\odot = 8.5$ Kpc, the distance of the Sun from the galactic centre and $\rho_\odot = 0.4$ GeV/cm^3 is the DM halo density at the position of the solar system. The expression of the annihilation cross-section $\langle\sigma v\rangle_{\text{SS}\to\gamma\gamma}$ (in eq. (22)) for the process shown in figure 9 is given in ref. [34]. In this calculation, we have considered three different DM halo profiles (available in literature), namely the Einasto profile [35], the NFW profile [36] and the isothermal profile [37]. These halo profiles give the functional dependence of $\rho(r)$ with r. In the present calculation, we have considered the value of the coupling $\delta_2 = 0.06$, which is allowed by WMAP and all recent ongoing DM direct detection experiments that have been considered in this work (figure 4). We have calculated the γ-ray fluxes for all the three halo profiles considered above and the results are shown in table 1. The annihilation cross-section $\langle\sigma v\rangle_{\text{SS}\to\gamma\gamma}$ is calculated to be 7.13×10^{-31} cm^3/s for $\delta_2 = 0.06$. From ref. [31], one sees that the γ-ray flux obtained from 'central region' of our galaxy is in the range 4.0×10^{-5}–7.5×10^{-5} GeV cm^{-2} s^{-1} sr^{-1} (95% CL) with best fit value, 5.6×10^{-5} GeV cm^{-2} s^{-1} sr^{-1}. From table 1, we see that in order to compare our results with those in ref. [31], the annihilation cross-section for the channel $SS \to \gamma\gamma$ in the present calculation must be enhanced by a factor of $\sim 3.0 \times 10^2$ (for the Einasto profile) and $\sim 5.7 \times 10^2$ (for the NFW profile) with respect to the best-fit value. As a result, we have to increase coupling δ_2 from 0.06 to 1.03 (for the Einasto profile) and

Table 1. γ-ray flux obtained from the annihilation channel $SS \rightarrow \gamma\gamma$ for three different dark matter halo profiles.

Mass of scalar DM (GeV)	Coupling δ_2	Flux using Einasto profile (GeV cm^{-2} s^{-1} sr^{-1})	Flux using NFW profile (GeV cm^{-2} s^{-1} sr^{-1})	Flux using isothermal profile (GeV cm^{-2} s^{-1} sr^{-1})
130	0.06	1.971×10^{-7}	9.801×10^{-8}	4.048×10^{-9}

1.43 (for the NFW profile), respectively. From figure 4, it is seen that such a high value of δ_2 is not satisfied by either any direct detection experiment we have considered in this work or by the WMAP limits. Therefore, we conclude that a 130 GeV DM in the present model cannot explain the Fermi-LAT-observed 130 GeV γ-ray line in the direction of the galactic centre unless the process is boosted (by introducing a boost factor [38]) either by astrophysical justifications and/or by other particle physics methods.

9. Summary and conclusion

In the present work, we consider the simplest extension of SM by introducing a real gauge singlet (singlet under $SU(2)_{\mathrm{L}} \times U(1)_{\mathrm{Y}}$) scalar S to SM which can only interact with SM particles via Higgs. For the stability of S, Z_2 symmetry is imposed in the theory. Thus, S can be a viable candidate for CDM. The scalar mass m_{S} and the coupling are the two parameters in the theory. We have calculated the freeze-out temperature and relic density of this scalar DM candidate S by solving Boltzmann's equation and have constrained the m_{S}–δ_2 parameter space by using WMAP limit on relic density of DM in the Universe and the results of recent ongoing DM direct search experiments such as CDMS-II, DAMA, CoGeNT, XENON-10 and XENON-100. We find that if S is a DM candidate, then its mass appears to be constrained within two regions. One is the lower mass region, where m_{S} can vary from 6 GeV to 16 GeV with δ_2 lying in the limit $0.7 \leq \delta_2 \leq 1.25$ for $m_{\mathrm{h}} = 120$ GeV. This region is supported by WMAP, CoGeNT and DAMA data. The other region is the higher mass region with the ranges for m_{S} (in GeV) and δ_2 found out to be $52.5 \lesssim m_{\mathrm{S}} \lesssim 1000$, $0.02 \leq \delta_2 \leq 0.4$ for the same Higgs mass. This region is also supported by the limits given by WMAP, CDMS-II, XENON-10, XENON-100 and EDELWEISS-II experiments. We have calculated the possible differential direct detection rates and annual variations of total detection rates for scalar DM S in the case of two detector materials, namely Ge and Xe. For these target materials, we have found that differential detection rates decrease rapidly with the increase of observed recoil energy and they become vanishingly small for recoil energies beyond 10 keV for Ge with scalar mass $m_{\mathrm{S}} = 10$ GeV, whereas for Xe, the rates become vanishingly small for recoil energies beyond 80 keV when $m_{\mathrm{S}} = 55$ GeV. We have also shown how the total rates vary over a year for these target materials. These annual variations of total detection rates, if found, will be a definite evidence for DM detection. Finally, in the last section, we have calculated the γ-ray flux for a 130 GeV scalar DM S and found that it is not possible to explain the Fermi-LAT-observed excess γ-ray line by a 130 GeV scalar DM, unless a boost

factor of the order of 10^2 is introduced with the annihilation cross-section of $SS \to \gamma\gamma$ channel.

Acknowledgement

The author AB thanks Debabrata Adak for some valuable discussions.

References

[1] WMAP Collaboration: D N Spergel *et al*, *Astrophys. J. Suppl.* **170**, 377 (2007)
WMAP Collaboration: E Komatsu *et al*, *Astrophys. J. Suppl.* **180**, 330 (2009)
[2] D E McLaughlin, arXiv:astro-ph/9812242
[3] E L Lokas and G A Mamon, *Mon. Not. R. Astron. Soc.* **343**, 401 (2003), arXiv:astro-ph/0302461
[4] M Bradac, *Nucl. Phys. Proc. Suppl.* **194**, 17 (2009)
[5] V Silveira and A Zee, *Phys. Lett.* **B161**, 136 (1985)
[6] M C Bento, O Bertolami, R Rosenfeld and L Teodoro, *Phys. Rev.* **D62**, 041302 (2000), arXiv:astro-ph/0003350
J McDonald, *Phys. Rev. Lett.* **88**, 091304 (2002), arXiv:hep-ph/0106249
H Davoudiasl, R Kitano, T Li and H Murayama, *Phys. Lett.* **B609**, 117 (2005), arXiv:hep-ph/0405097
D O'Connell, M J Ramsey-Musolf and M B Wise, *Phys. Rev.* **D75**, 037701 (2007), arXiv:hep-ph/0611014
V Barger, P Langacker, M McCaskey, M J Ramsey-Musolf and G Shaughnessy, *Phys. Rev.* **D77**, 035005 (2008), arXiv:0706.4311 [hep-ph]
Carlos E Yaguna, *J. Cosmol. Astropart. Phys.* **0903**, 003 (2009), arXiv:0810.4267 [hep-ph]
X G He, T Li, X Q Li, J Tandean and H C Tsai, *Phys. Rev.* **D79**, 023521 (2009), arXiv:0811.0658 [hep-ph]
X G He, T Li, X Q Li, J Tandean and H C Tsai, *Phys. Lett.* **B688**, 332 (2010), arXiv:0912.4722 [hep-ph]
X G He, S Y Ho, J Tandean and H C Tsai, *Phys. Rev.* **D82**, 035016 (2010), arXiv:1004.3464 [hep-ph]
A Bandyopadhyay, S Chakraborty, A Ghosal and D Majumdar, *J. High Energy Phys.* **1011**, 065 (2010), arXiv:1003.0809 [hep-ph]
M Asano and R Kitano, *Phys. Rev.* **D81**, 054506 (2010), arXiv:1001.0486 [hep-ph]
[7] M H G Tytgat, arXiv:1012.0576 [hep-ph]
[8] S Andreas, T Hambye and M H G Tytgat, *J. Cosmol. Astropart. Phys.* **0810**, 034 (2008), arXiv:0808.0255 [hep-ph]
[9] The DAMA Collaboration: R Bernabei *et al*, *Eur. Phys. J.* **C56**, 333 (2008); *AIP Conf. Proc.* **698**, 328 (2004); *Int. J. Mod. Phys.* **D13**, 2127 (2004)
[10] The CoGeNT Collaboration: C E Aalseth *et al*, arXiv:1002.4703 [astro-ph.CO]
[11] The CDMS-II Collaboration: Z Ahmed *et al*, arXiv:0912.3592 [astro-ph.CO]
[12] S Andreas, C Arina, T Hambye, F S Ling and M H G Tytgat, *Phys. Rev.* **D82**, 043522 (2010), arXiv:1003.2595 [hep-ph]
[13] XENON 100 Collaboration: E Aprile *et al*, arXiv:1104.2549v2 [astro-ph.CO]
[14] A Liam Fitzpatrick, D Hooper and K M Zurek, arXiv:1003.0014 [hep-ph]
[15] A A Abdo *et al*, *Astrophys. J.* **712**, 147 (2010), arXiv:1001.4531 [astro-ph.CO]
[16] C Arina and M H G Tytgat, *J. Cosmol. Astropart. Phys.* **1101**, 011 (2011), arXiv:1007.2765 [astro-ph.CO]

C Balazs, N Sahu and A Mazumdar, *J. Cosmol. Astropart. Phys.* **0907**, 039 (2009), arXiv:0905.4302 [hep-ph]
K Kohri, J McDonald and N Sahu, *Phys. Rev.* **D81**, 023530 (2010), arXiv:0905.1312 [hep-ph]
C Arina, F-X Josse-Michaux and N Sahu, *Phys. Rev.* **D82**, 015005 (2010), arXiv:1004.3953 [hep-ph]

[16a] This is the only parameter in this model which appears in both the expressions of scattering and annihilation cross-section of S and which depends on the masses of scalar S and Higgs h.

[17] CDMS-II Collaboration: Z Ahmed *et al*, *Phys. Rev. Lett.* **106**, 131302 (2011), arXiv:1011.2482 [astro-ph.CO]

[18] XENON 10 Collaboration: J Angle *et al*, *Phys. Rev. Lett.* **100**, 021303 (2008), arXiv:astro-ph/0706.0039
E Aprile and T Doke, *Rev. Mod. Phys.* **82**, 2053 (2010)

[19] CoGeNT Collaboration, C E Aalseth *et al*, *Phys. Rev. Lett.* **107**, 141301 (2011), arXiv:1106.0650 [astro-ph.CO]

[20] EDELWEISS Collaboration: E Armengaud *et al*, arXiv:1103.4070v2 [astro-ph.CO]

[21] P Gondolo and G Gelmini, *Nucl. Phys.* **B360**, 145 (1991)

[22] J McDonald, *Phys. Rev.* **D50**, 3637 (1994), arXiv:hep-ph/0702143

[23] W-L Guo and Y-L Wu, *J. High Energy Phys.* **1010**, 083 (2010), arXiv:1006.2518 [hep-ph]

[23a] Physically, we can say that $\langle \sigma v \rangle$ is directly proportional to the probability of that process. So, for higher $\langle \sigma v \rangle$, the probability of pair annihilation of S is high and hence density is low.

[24] M Srednicki, R Watkins and K A Olive, *Nucl. Phys.* **B310**, 693 (1988)

[25] SIMPLE Collaboration: M Felizardo *et al*, arXiv:1106.3014 [astro-ph.CO]

[26] C P Burgress, M Pospelov and T ter Veldhuis, *Nucl. Phys.* **B619**, 709 (2001), arXiv:hep-ph/0011335

[27] G Jungman, M Kamionkowski and K Griest, *Phys. Rep.* **267**, 195 (1996), arXiv:hep-ph/9506380

[28] J Engel, *Phys. Lett.* **B264**, 114 (1991)

[29] A Bottino, V de Alfaro, N Fornengo, G Mignola and S Scolpel, *Astropart. Phys.* **2**, 77 (1994)

[30] C Weniger, *J. Cosmol. Astropart. Phys.* **1208**, 007 (2012), arXiv:1204.2797 [hep-ph]

[31] E Tempel, A Hektor and M Raidal, arXiv:1205.1045 [hep-ph]

[32] LAT Collaboration: W B Atwood *et al*, *Astrophys. J.* **697**, 1071 (2009), arXiv:0902.1089 [astro-ph.IM]

[33] LAT Collaboration: M Ackermann *et al*, arXiv:1205.2739 [astro-ph.HE]

[34] S Profumo, L Ubaldi and C Wainwright, *Phys. Rev.* **D82**, 123514 (2010), arXiv:1009.5377 [hep-ph]

[35] J Einasto, *Trudy Inst. Astrofiz. Alma-Ata* **5**, 87 (1965)
J F Navarro *et al*, *Mon. Not. R. Astron. Soc.* **349**, 1039 (2004), astro-ph/0311231

[36] J F Navarro, C S Frenk and S D M White, *Astrophys. J.* **490**, 493 (1997), astro-ph/9611107

[37] J N Bahcall and R M Soneira, *Astrophys. J. Suppl.* **44**, 73 (1980)

[38] A Sommerfeld, *Annalen der Physik* **403**, 257 (1931)
N Arkani-Hamed, D P Finkbeiner, T R Slatyer and N Weiner, *Phys. Rev.* **D79**, 015014 (2009), arXiv:0810.0713 [hep-ph]
Q-H Cao, I Low and G Shaughnessy, *Phys. Lett.* **B691**, 73 (2010), arXiv:0912.4510 [hep-ph]